Module-Integrated Converter Based on Cascaded Quasi-Z-Source Inverter With Differential Power Processing Capability for Photovoltaic Panels Under Partial Shading

Masatoshi Uno, *Member, IEEE*, and Toshiki Shinohara

(Highlighted Paper)

***Abstract*—Conventional microinverter or module-integrated converter (MIC)-based photovoltaic (PV) systems are prone to be complex and costly because each MIC requires not only a boost converter to bridge a huge voltage gap between a PV panel and grid but also desirably a differential power processing (DPP) converter to preclude partial shading issues. This paper proposes a novel MIC based on cascaded quasi-Z-source inverters (qZSIs) with DPP capability. A traditional qZSI and voltage multiplier (VM)-based DPP converter are integrated into a single unit with sharing active switches and magnetic components, achieving system- and circuit-level simplifications. In addition, a novel control strategy utilizing two control freedoms of shoot-through duty cycle d_{st} and modulation index *M* to simultaneously perform maximum power point tracking (MPPT) and DPP function, respectively, is also presented. A 150 W prototype for a standard PV panel consisting of three substrings is built, and experimental tests are performed emulating partial shading conditions. The results demonstrate that the proposed integrated qZSI could perform MPPT with satisfactory preventing partial shading issues while generating ac voltage at the inverter output.**

***Index Terms*—Differential power processing (DPP) converter, module-integrated converter (MIC), partial shading, photovoltaic system, quasi-Z-source inverter (qZSI).**

I. Introduction

MICROINVERTER or module-integrated converter (MIC)-based power conversion has become an important trend in photovoltaic (PV) systems. Each PV panel is installed with an MIC, allowing flexible system design and good scalability of the PV system because the number of panels can be arbitrarily extended by installing PV panels with MICs, without redesigning power conversion electronics.

Manuscript received August 11, 2018; revised December 3, 2018 and February 14, 2019; accepted March 14, 2019. Date of publication March 18, 2019; date of current version September 6, 2019. This work was supported in part by Power Academy. Recommended for publication by Associate Editor J. H. R. Enslin. *(Corresponding author: Masatoshi Uno.)*

M. Uno is with the College of Engineering, Ibaraki University, Hitachi 316-8511, Japan (e-mail:

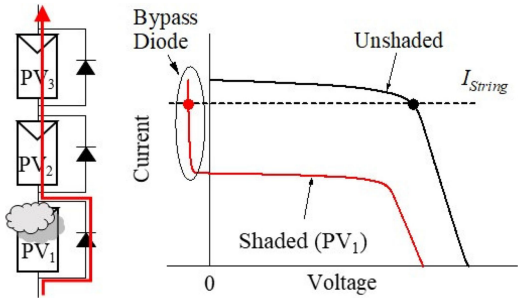

Fig. 1. Shaded and unshaded substrings in PV panel.

precluded [21]. Partial shading on a PV panel/string (hereafter, call string) comprising multiple substrings connected in series triggers characteristic mismatch of substrings, as shown in Fig. 1. The shaded substring, which is less capable of producing current, is bypassed by a parallel-connected bypass diode, and therefore, its voltage is subzero value. Since the shaded substring no longer produces power, the power generation of the string as a whole significantly drops. In addition to the reduced power yield, multiple power point maxima appear on string's *P–V* characteristic that hinders and confuses ordinary maximum power point tracking (MPPT) algorithms.

To preclude such partial shading issues, various kinds of differential power processing (DPP) converters or voltage equalizers (hereafter called DPP converters unless otherwise noted) have been proposed and developed [22]–[44]. With DPP converters, a fraction of generated power of unshaded substrings is redistributed to shaded ones so that all substrings can operate at the same voltage or even at each MPP. All substring characteristics, including not only unshaded substrings but also shaded ones, can be virtually unified by DPP converters, and hence the string can behave as if there is no partial shading.

Depending on power redistribution strategies, DPP converter architectures can be categorized into several groups, as shown in Fig. 2, in which a boost converter before an inverter stage is also illustrated. The adjacent substring DPP architecture [see Fig. 2(a)] is based on nonisolated bidirectional converters, such as pulse width modulation converters [23]–[27], multi-stage choppers [28], [29], and switched capacitor converters [30]–[33], through which neighboring two substrings transfer power each other. String-to-substring DPP architectures employ either a single-input–multi-output converter [34]–[38] [Fig. 2(b)] or multiple isolated bidirectional flyback converters [39], [40] [Fig. 2(c)] to provide power transfer paths between a string and substrings. The substring-to-bus architecture [44] [Fig. 2(d)] is very similar to the string-to-substring one but its power transfer is between a bus and substrings. In the substring-to-isolated port (IP) DPP architecture with a virtual bus [39]–[43], any substrings can directly exchange power through the IP.

A conventional PV MIC system with a string-to-substring DPP converter is illustrated in Fig. 3, as a representative configuration. Although the partial shading issues can be prevented by DPP converters, three converters (i.e., the boost converter, inverter, and DPP converter) are separately necessary, increasing the system complexity and cost. If these three converters were to be integrated into a single unit with reducing passive and active

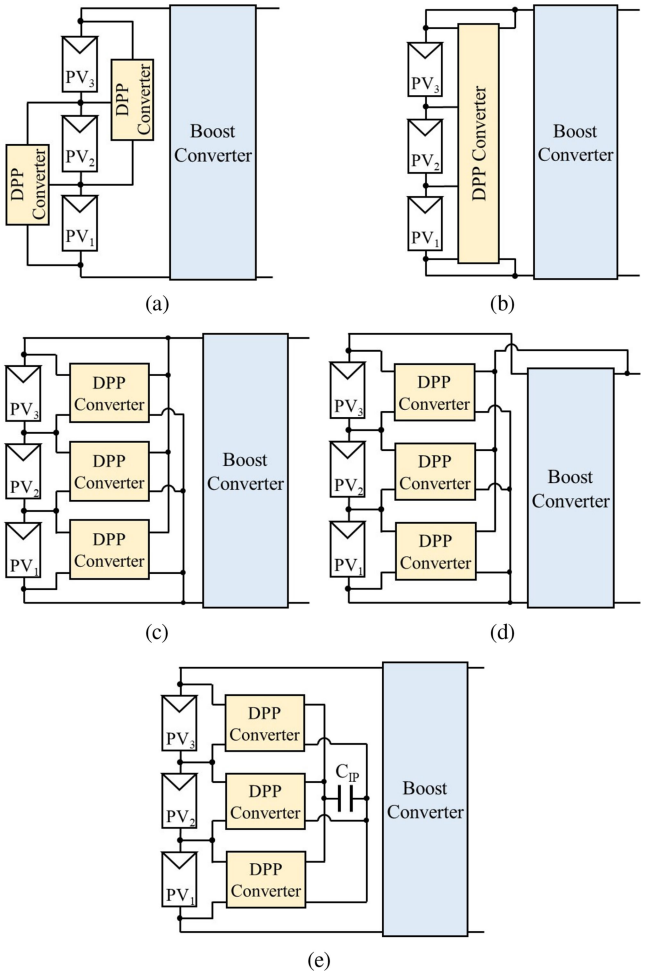

Fig. 2. DPP converter system architectures. (a) Adjacent substring (PV-to-PV). (b) String-to-substring with single-input–multi-output converter. (c) String-to-substring with multiple converters. (d) Substring-to-bus. (e) Substring-to-IP (virtual bus).

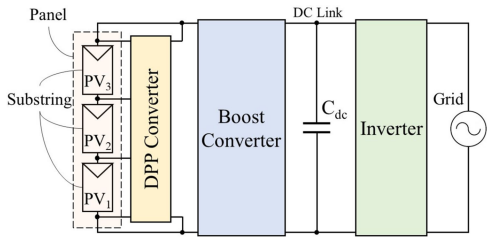

Fig. 3. Conventional MIC system with DPP converter.

devices, the PV MIC system would potentially be simpler and less expensive.

To achieve simplified PV systems, the qZSI integrating a DPP converter has been proposed in our prior work [45]. This paper presents the extended and fully developed work of [45]. The notional PV MIC system using the proposed integrated qZSI is shown in Fig. 4. The proposed integrated qZSI is based on the combination of a traditional qZSI and a voltage multiplier (VM)-based string-to-substring DPP converter [37], [38]. A qZSI and VM-based DPP converter are integrated into a single unit with reducing active switches and magnetic components, hence contributing to reduced circuit complexity and cost. This paper

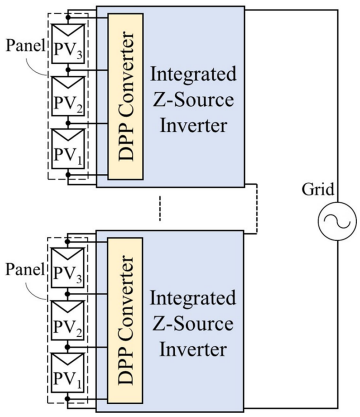

Fig. 4. Proposed PV MIC based on cascaded qZSIs integrating DPP converter.

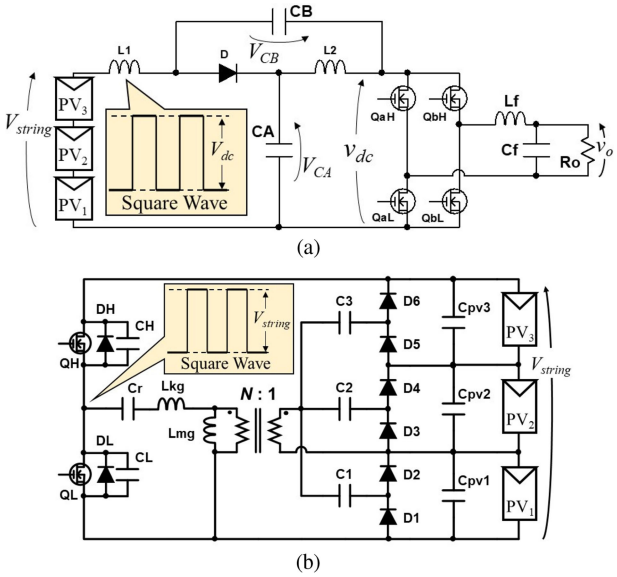

Fig. 5. Key circuits for integrated qZSI. (a) qZSI. (b) VM-based DPP converter.

is organized as follows. The derivation procedure and major features of the integrated qZSI are discussed in Section II, followed by the operation analysis in Section III. A control strategy to perform both MPPT and DPP function will be presented in Section IV. Section V shows experimental results performed emulating partial shading conditions.

II. Proposed Integrated Quasi-Z-Source Inverter

A. Key Circuits for Integrated Quasi-Z-Source Inverter

The proposed integrated qZSI is derived from the combination of two key circuits of a traditional qZSI and VM-based DPP converter, as shown in Fig. 5(a) and (b), respectively.

The qZSI is the foundation of the proposed circuit. The dc-link voltage $v_{\rm dc}$ in the qZSI is zero during ST states, in which both the high- and low-side switches are simultaneously on. During active and zero states, $v_{\rm dc}$ is at its high level of $V_{\rm dc}$. Hence, $v_{\rm dc}$ swings with a peak-to-peak voltage of $V_{\rm dc}$. At the same time, voltages across inductors also swing with a peak-to-peak value of $V_{\rm dc}$, generating square wave voltages across inductors, as shown in the inset of Fig. 5(a). In general, a voltage gain of qZSIs is dependent on two control degrees of freedom: an ST duty cycle d_{st} and modulation index M [4], [19]. A boost factor, which is the ratio of $V_{\rm dc}$ to an input voltage, is dependent on d_{st}. Meanwhile, M dictates the relationship between $V_{\rm dc}$ and output peak phase voltage of the inverter.

The DPP converter using a VM [shown in Fig. 5(b)] has been proposed as a simple voltage equalizer for PV panels to preclude partial shading issues [37], [38]. The VM is driven by a square wave voltage generated by a leg consisting of Q_H and Q_L [as depicted in the inset of Fig. 5(b)], and equalization currents are automatically supplied to shaded substrings even without feedback control. The detailed automatic equalization mechanism is found in [37], [38].

B. Derivation of Proposed Integrated qZSI

The proposed integrated qZSI can be derived from the combination of the key circuits shown in Fig. 5. By utilizing the square wave voltage produced across L_1 in the traditional qZSI to drive the VM-based DPP converter, the two circuits can be integrated into a single unit with eliminating some key circuit elements, as shown in Fig. 6. L_1 in the traditional qZSI is replaced with the transformer primary winding of the VM-based DPP converter. The VM consisting of capacitors and diodes is connected to the transformer secondary winding and is essentially switchless. The structure of the VM can be applied to an arbitrary number of substrings connected in series by simply stacking capacitor–diode network in the VM, as reported in the previous work [37].

The magnetizing inductance of the transformer L_{mg} behaves as an inductor L_1 in the traditional qZSI. The resonant capacitor C_r in the conventional VM-based DPP converter [see Fig. 5(b)] is removed not to block a dc current component in the primary winding. As $v_{\rm dc}$ swings, a square wave voltage is generated across the primary winding, by which the secondary circuit of the VM is driven.

As mentioned in Section II-A, there are two control freedoms of d_{st} and M in conventional qZSIs. In the proposed integrated qZSI, d_{st} is used for MPPT of the PV string, while the DPP converter is controlled with M. The details about the control strategy will be discussed in Section IV.

C. Major Features

In comparison with the conventional PV MIC system shown in Fig. 3, three separate converters (the boost converter, inverter, and DPP converter) are integrated into a single unit, contributing to the simplified system and potentially reducing the cost. In addition, the circuit-level simplification is also feasible because the DPP converter in the integrated qZSI is essentially switchless—the VM circuit is driven by the square wave voltage generated in the qZSI.

In contrast, the major drawback is that individual performances as a qZSI and DPP converter cannot be optimized due to the integration. More precisely, the qZSI and VM share the transformer primary winding, and its operation can never be optimized for both circuits. Hence, the proposed integrated qZSI is considered suitable for relatively low-power applications where

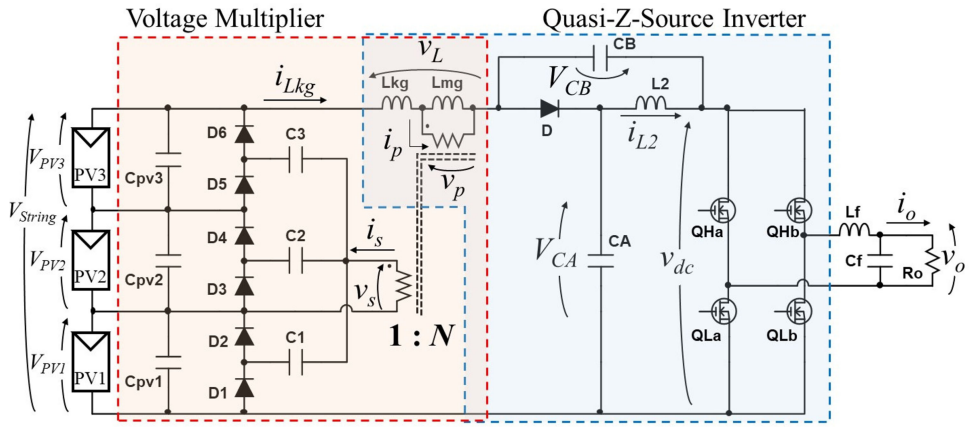

Fig. 6. Proposed integrated qZSI for three substrings.

system simplification and cost reduction are prioritized over performance optimization.

In general, a square wave voltage is produced in any inverters, including extended versions of ZSIs [8]–[18], and the integration concept of the proposed qZSI can be applied to other types of ZSIs, potentially generating novel integrated inverter topologies—a search for novel topologies will be a part of our future works.

D. Qualitative Comparison With Conventional DPP Converter Systems

The proposed integrated qZSI is qualitatively compared with conventional DPP architectures listed in Fig. 2, from the viewpoint of complexity, voltage stress of switches, scalability, and efficiency. Since the VM-based DPP converter in the proposed integrated qZSI is categorized into the string-to-substring DPP architecture [Fig. 2(b)], major benefits and drawbacks of the string-to-substring architecture are inherited to the proposed qZSI.

Complexity: The conventional DPP architectures, except for the string-to-substring architecture [Fig. 2(b)], require multiple DPP converters each having at least two switches for bidirectional power flow, hence increasing the system and circuit complexities. In the string-to-substring DPP architecture, on the other hand, one single DPP converter with less than two switches handles all substrings, achieving the simplified system by reducing the DPP converter count. The VM-based DPP converter in the proposed integrated qZSI is essentially switchless (see Fig. 6), hence realizing the further circuit simplification.

Voltage stress of switches: DPP converters in Fig. 2(b)–(d) are connected to a string or bus, and therefore their switches must be rated for relatively high voltage. On the other hand, switches with low voltage rating can be used for the adjacent and substring-to-IP DPP converters. Meanwhile, the VM-based DPP converter in the proposed qZSI is switchless, and therefore, the switch voltage rating is no longer an issue.

Scalability: Architectures using multiple DPP converters [Fig. 2(a), (c)–(e)] can be flexibly scaled up for large PV systems by adding DPP converters. On the other hand, the DPP converters in the string-to-substring architecture [Fig. 2(b)] and the proposed qZSI need to be redesigned for different number of substrings, impairing the scalability.

Efficiency: Power conversion efficiency of individual DPP converters is reportedly 85–95%. However, an overall efficiency is more dependent on DPP architectures and system scale rather than individual converter efficiencies. Power transfer in the adjacent DPP architecture is limited only between neighboring substrings, and power conversion losses might be collectively large in a long string. The substring-to-IP architecture [Fig. 2(e)] realizes direct power transfer among substrings, but it is essentially based on two-stage power conversion via the IP. DPP architectures of Fig. 2(b)–(d) allow direct power transfer between a substring and string or bus without multi-stage power conversion. Overall efficiencies would be maximized in the DPP systems allowing bidirectional power flow [Fig. 2(c) and (d)] by minimizing processing power.

E. Extended Topology for Higher Step-Up Voltage Conversion Ratio

The step-up ratio of the proposed qZSI is practically limited to less than 2.0 due to limitations of duty cycle d_{st} and modulation index M, similar to ordinary qZSIs [7]. To achieve higher step-up voltage conversion ratios, extended ZSI topologies can be employed as a foundation of the proposed integrated qZSI concept, as exemplified in Fig. 7. In this example, a capacitor-assisted qZSI [8] is used as the foundation that realizes twice higher voltage gain than does the basic topology shown in Fig. 6, while the transformer is shared by the capacitor-assisted qZSI and VM. Other extended ZSI topologies [8]–[18] can also be employed by replacing one of the inductors in ZSIs with a transformer. A proper topology should be selected with considering voltage step-up requirement and design difficulty.

F. Leakage Current Suppression and Isolated Micro-Inverter Applications

The conventional qZSIs, including the proposed integrated qZSI, are transformerless topologies and may introduce leakage current issues due to the common-mode voltage. The past

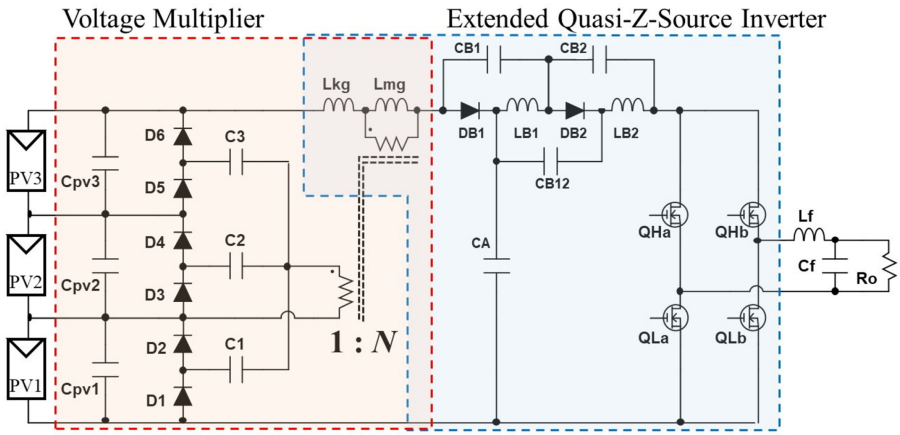

Fig. 7. Extended topology of proposed integrated qZSI for higher step-up ratio.

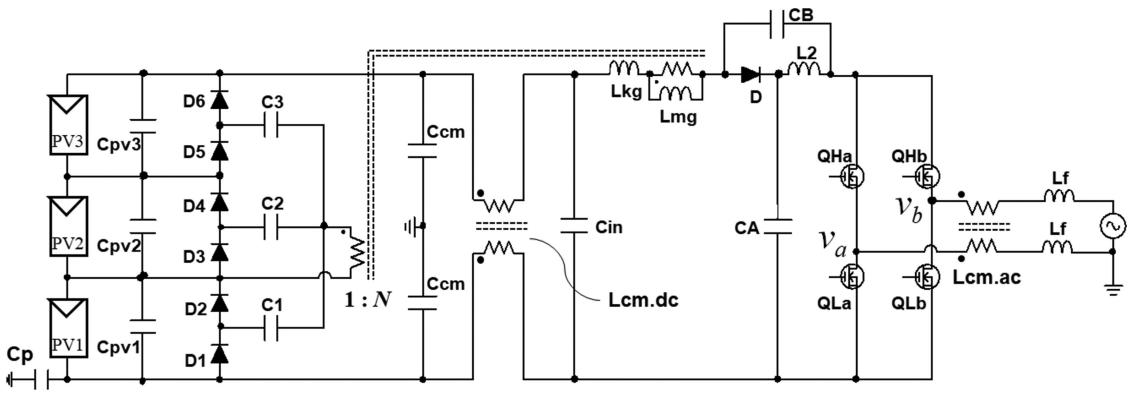

Fig. 8. Integrated qZSI with ac- and dc-side common mode chokes and common mode capacitors to suppress leakage current originating from parasitic capacitor.

work about the cascaded qZSI system [20] discusses the leakage current suppression issue and refers to [46] that the filter-based solution will help to suppress leakage current through employing common mode (CM) chokes, CM capacitors, and ac-side CM chokes, as shown in Fig. 8. A circulating leakage current loop is formed due to a grounding point and a parasitic capacitance C_p between the PV panel and the earth. The common mode voltage $v_{\rm CM}$ is defined as $(v_a + v_b)/2$ where v_a and v_b are the phase-leg voltages as designated in Fig. 8. The filter consisting of the ac- and dc-side CM chokes of $L_{\rm cm.ac}$ and $L_{\rm cm.dc}$, filter inductor L_f, and CM capacitors $C_{\rm cm}$ is designed to lessen the high-frequency harmonics across C_p so that the leakage current is suppressed. The detailed analysis and results of experimental verifications can be found in [46].

To adequately preclude the leakage current issues, transformer-based isolated converters with galvanic isolation, such as flyback converter [47], forward converter [3], and cycloconverter [48], would be a better option. In such isolated converters, a square wave voltage is generated across transformer windings, hence driving expectations that the concept of the proposed integration may potentially be applied through the transformers. A search for feasible isolated micro-inverter topologies with integrated DPP capability will be a part of our future works.

III. Operation Analysis

A. Fundamental Operation

In this section, the fundamental operating principle is explained with an example case where $\rm PV_1$ is partially-shaded. All circuit elements are assumed ideal. Although a simple boost control method is employed throughout this paper, other modulation methods, such as maximum constant boost control and space vector modulation, can be applied to the integrated qZSI.

Key operation waveforms and current flow directions in a single switching cycle are shown in Figs. 9 and 10, respectively. It is noted that the inverter leg is depicted as a current source or short-circuit depending on switching states. According to switching patterns of qZSIs, there are an ST, active, and zero states. The current flow path in the ST state corresponds to those in Modes 1 and 2. Modes 3 and 4, on the other hand, represent active or zero states.

Mode 1 [Fig. 10(a)]*:* Both the high- and low-side switches are on in this ST state, and $v_{\rm dc}$ is zero. The currents of L_{mg} and $\rm L_2$, $i_{\rm Lmg}$ and i_{L2}, decrease and increase linearly, respectively. The voltage across the transformer primary winding v_L is equal to $V_{\rm string} + V_{CB} = V_{CA}$ [see (8)]. On the transformer secondary side, the current i_s flows through $\rm C_1$ and $\rm D_1$, the low-side diode that is connected in parallel with the shaded substring $\rm PV_1$.

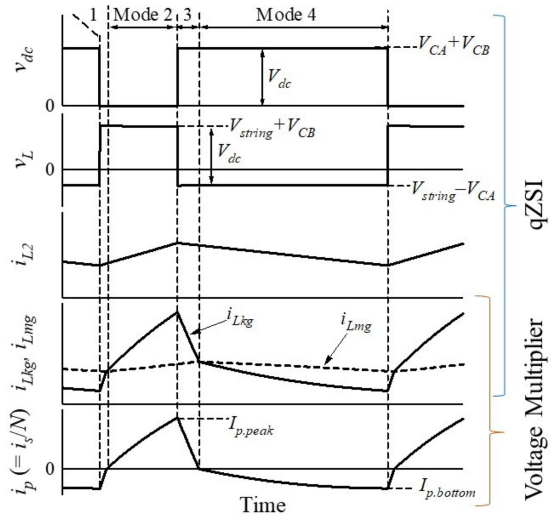

Fig. 9. Key operation waveforms when PV_1 is partially shaded.

i_s is reflected on the primary side in the form of $i_p\,(=i_s/N)$ and is superimposed on i_{Lmg}, becoming i_{Lkg}.

Mode 2 [Fig. 10(b)]*:* This mode begins as i_s becomes positive. In the VM, i_s flows through D_2, the high-side diode connected in parallel with the shaded substring. i_s and i_{Lkg} show a typical LR response that reflects L_{kg} and collective resistance in the current path. Both L_{mg} and L_2 store energy and their currents increase.

Mode 3 [Fig. 10(c)]*:* This mode corresponds to active or zero states. i_{Lmg} still linearly increases, whereas L_2 starts discharging through the diode D and its currents i_{L2} linearly decreases. v_{dc} is at a high level, and its peak value is equal to the sum voltage $V_{CA}+V_{CB}$. v_L is $V_{string}-V_{CA}=-V_{CB}$ [see (8)] and its polarity is negative. On the transformer secondary side, i_s keeps flowing through D_2 but it sharply decreases.

Mode 4 [Fig. 10(d)]*:* This mode starts as i_s and becomes negative in active or zero states. The low-side diode D_1 conducts again. Both i_{Lmg} and i_{L2} decrease. This mode lasts until the inverter leg is short-circuited.

Assuming the collective resistance in the current path is negligibly low and both i_{Lkg} and i_{Lmg} change linearly, the current flowing through the primary winding, i_p, is expressed as

$$i_p = i_{Lkg} - i_{Lmg} = \left(\frac{v_L - v_p}{L_{kg}} - \frac{v_p}{L_{mg}}\right) t = \left\{\frac{v_L}{L_{kg}} - \left(\frac{L_{kg}+L_{mg}}{L_{kg}L_{mg}}\right) v_p\right\} t. \quad (1)$$

The voltage across L_{kg} and L_{mg}, v_L, is

$$v_L = \begin{cases} V_{CA} & \text{(Modes 1 and 2)} \\ -V_{CB} & \text{(Modes 3 and 4).} \end{cases} \quad (2)$$

The voltage of the primary winding, v_p, is

$$v_p = \begin{cases} N\left(V_{C1} - V_{PV1} - V_f\right) & \text{(Modes 1 and 4)} \\ N\left(V_{C1} + V_f\right) & \text{(Modes 2 and 3).} \end{cases} \quad (3)$$

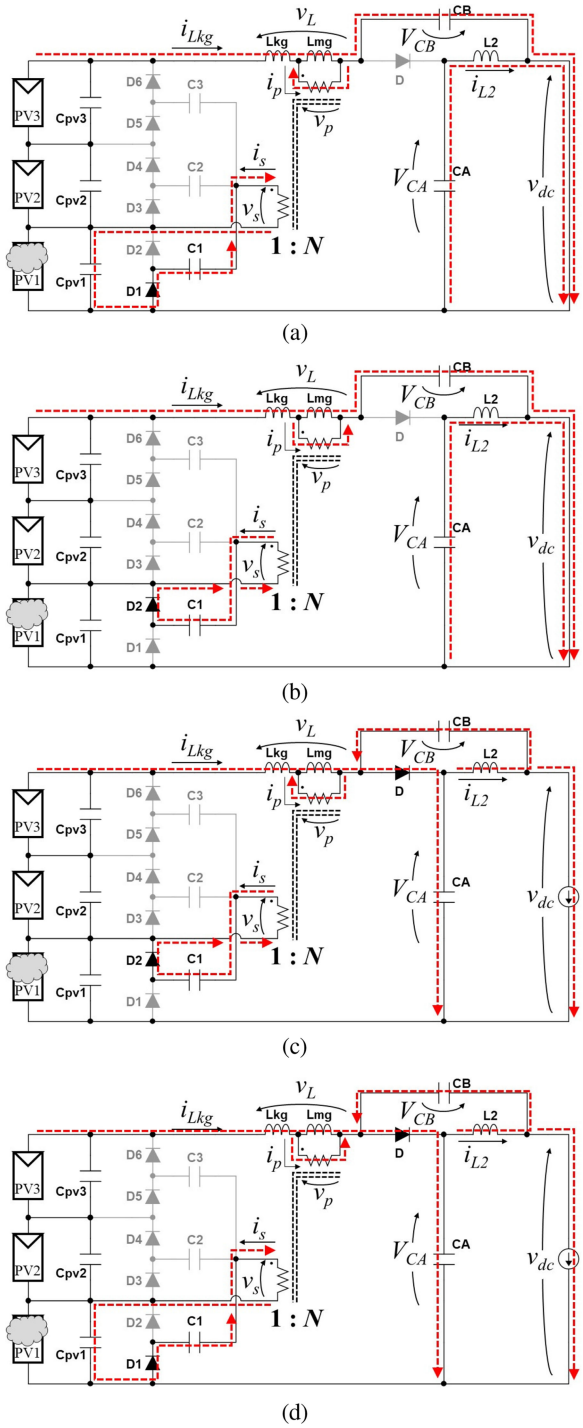

Fig. 10. Operation modes when PV_1 is shaded in (a) Mode 1, (b) Mode 2, (c) Mode 3, and (d) Mode 4.

where V_{C1} is the average voltage of C_1, and V_f is the forward voltage of diodes in the VM.

Modes 1 and 3 are short enough to be neglected, and therefore, duty cycles of D_1 and D_2 can be approximated to be $1-d_{st}$ and d_{st}, respectively. The average voltage of the mid-point of D_1 and D_2 is $d_{st}V_{PV1}$. Since the average voltage of the transformer secondary winding must be zero under steady-state conditions,

$$V_{C1} = (1-d_{st})\,V_{PV1}. \quad (4)$$

Assuming $V_f = 0$ for the sake of clarity, substitution of (2)–(4) into (1) produces the peak value of i_p, $I_{p.peak}$, as

$$I_{p.\mathrm{peak}} = \left\{ \frac{V_{CA}}{L_{kg}} - N \left(\frac{L_{kg} + L_{mg}}{L_{kg} L_{mg}} \right) (1 - d_{st}) V_{PV1} \right\} \frac{d_{st} T_s}{2}. \tag{5}$$

where d_{st} is the ST duty cycle, T_s is the switching period. From the charge balance on C_1, the bottom value of i_p, $I_{p.bottom}$ is

$$I_{p.\mathrm{bottom}} = \frac{d_{st}}{1 - d_{st}} I_{p.\mathrm{peak}}. \tag{6}$$

In summary, v_L swings and its peak-to-peak voltage is equal to that of v_{dc}, V_{dc}, as designated in Fig. 9. At the same time, a square wave voltage with the peak-to-peak voltage of V_{dc}/N appears across the secondary winding, by which the VM is driven. In the VM, D_1 and D_2 that are connected in parallel with the shaded substring PV_1, are in operation, whereas others do not conduct for the entire period, meaning only the shaded substring receives the current from the VM. Since the average current of C_1 must be zero under steady-state conditions, the average current of D_1 or D_2 is equal to the current supplied to the shaded substring from the VM. Although the PV_1-shaded condition was taken as an example case, the VM in the proposed integrated qZSI can operate similarly under any shading conditions, as reported in the previous work [37].

B. Quasi-Z-Source Inverter

The operation principle of the qZSI in the proposed circuit is essentially identical to that of traditional ones. The peak value of the dc-link voltage v_{dc}, V_{dc}, is expressed as [49]

$$V_{\mathrm{dc}} = \frac{V_{\mathrm{string}}}{1 - 2d_{st}} = V_{CA} + V_{CB} \tag{7}$$

where V_{string} is the string voltage. V_{CA} and V_{CB} are given by [19]

$$V_{CA} = \frac{1 - d_{\mathrm{st}}}{1 - 2d_{\mathrm{st}}} V_{\mathrm{string}}, \quad V_{CB} = \frac{d_{\mathrm{st}}}{1 - 2d_{\mathrm{st}}} V_{\mathrm{string}}. \tag{8}$$

Equation (7) suggests that, at a given value of V_{dc}, V_{string} is controllable and MPPT is feasible with manipulating d_{st}.

The output peak phase voltage of the qZSI, V_o, is given by

$$V_o = M V_{\mathrm{dc}} \tag{9}$$

where M is the modulation index. This equation means that the peak dc-link voltage V_{dc} can be arbitrarily determined by adjusting M at a given value of V_{o}. As will be discussed in detail in the next section, the operation criterion of the VM in the integrated qZSI is dependent on V_{dc}, and therefore, M is used to control the VM-based DPP converter.

Under unshaded conditions, no currents from the VM flow toward substrings. The current of the secondary winding $i_s (= N i_p)$ is zero, and therefore, i_{Lkg} is equal to i_{Lmg}. Since the VM is inactive under unshaded conditions, the proposed integrated qZSI just operates as an ordinary qZSI. It suggests that, except for the part of the VM-based DPP converter, the proposed integrated qZSI can be designed identically to traditional ones. Current and voltage stresses of a traditional qZSI are summarized in [50]. Under shaded conditions, on the other hand, the peak value of i_{Lkg} tends to be high due to the operation of the VM-based DPP converter, as can be seen in Fig. 9. From the derived $I_{p.\mathrm{peak}}$ (5) with the generalized current stresses of the traditional qZSI [50], current stresses in the proposed integrated qZSI can be determined.

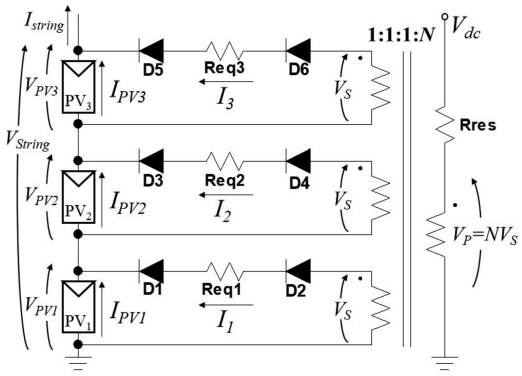

Fig. 11. DC equivalent circuit of VM-based DPP converter.

C. Voltage Multiplier-Based DPP Converter

The detailed operation of the VM-based DPP converter alone has been thoroughly analyzed in the past works [37], [38]. As discussed in Section III-A, the capacitor C_1, which corresponds to the shaded substring, is charged and discharged, and its operation can be expressed using an equivalent resistance.

The dc equivalent circuit of the VM-based DPP converter is shown in Fig. 11 [37]. R_{eq1}–R_{eq3} are equivalent resistors that represent the charge–discharge operation of capacitors C_1–C_3, and R_{res} is an equivalent resistance of the circuit on the primary side. Values of R_{eq} and R_{res} are inversely proportional to capacitances and switching frequency [37], [38]. The primary winding of the ideal multi-winding transformer is connected to the voltage source, and its value is equal to the peak-to-peak voltage of v_L. Hence, in the integrated qZSI, its value is V_{dc} because the peak-to-peak voltage of v_L is equal to V_{dc}, as explained in Section III-A.

All the substrings are connected to the secondary winding of the ideal multi-winding transformer through two diodes and a respective equivalent resistor. In order for the VM to supply equalization currents $I_i (i = 1 \ldots 3)$ for shaded substrings, V_{dc} needs to fulfill the following relationship:

$$V_{\mathrm{dc}} > N \left(V_{\mathrm{PV}} + 2V_f \right) \tag{10}$$

where V_{PV} is the substring voltage. From (9) and (10), the operation criterion of the VM-based DPP converter in the integrated qZSI is obtained as

$$M < \frac{V_o}{N \left(V_{PV} + 2V_f \right)}. \tag{11}$$

This equation suggests that the VM-based DPP converter can be enabled/disabled by properly manipulating M depending on partial shading conditions. When the DPP converter is enabled by setting M low, an equalization current I_i automatically flows toward shaded substring(s) having the lowest voltage in the string.

TABLE I
COMPONENT VALUES USED FOR THE PROTOTYPE

Component	Value
C_{ext}	Aluminum Electrolytic Capacitor, 330 μF × 6
C_A, C_B	Aluminum Electrolytic Capacitor, 1 mF × 4
L_2	150 μH
Switches	BSC320N20NS3, R_{on} = 32 mΩ
Diode	Fast Recovery Diode, BVY29, V_F = 1.05 V
Transformer	N_1:N_2 = 22:4, L_{kg} = 7.8 μH, L_{mg} = 263 μH
C_1–C_3	Ceramic Capacitor, 22 μF × 3
C_{pv1}–C_{pv3}	Ceramic Capacitor, 47 μF × 4
D_1–D_4	Schottky Barrier Diode, SL42, V_F = 0.47 V
Gate Driver	IRS2186

D. Design of Transformer and Voltage Multiplier-Based DPP Converter

This section presents a design example of the transformer as well as the VM-based DPP converter for the proof-of-concept prototype (see Table I in Section V) with operation constraints of $d_{st} < 0.3$ and $M < 1 - d_{st}$ for $V_o = 50$ V at $f_s = 20$ kHz. All substring voltages are assumed to be equal to $V_{PV} = 12$ V.

The transformer turns ratio N is determined from (11), as

$$N < \frac{V_o}{M\,(V_{PV} + 2V_f)} = 5.52 \rightarrow 5.5 \tag{12}$$

where $V_f = 0.47$. Since $L_{\rm mg}$ corresponds to L_1 in ordinary qZSIs [see Fig. 5(a)], the number of turns should be properly determined to have a desired inductance value of $L_{\rm mg}$.

As can be seen in Fig. 10, $L_{\rm kg}$ and a capacitor in the VM (i.e., C_1 in the case of $\rm PV_1$-shaded condition) might resonate, depending on operating conditions. The VM-based DPP converter can be driven in either resonant or nonresonant mode. The conventional VM-based DPP converter is driven with a duty cycle of 0.5 and is suitable for resonant operations [37]. The DPP converter in the integrated qZSI, on the other hand, operates with $d_{st} < 0.3$, and the resonance leads to a higher peak and root mean square (rms) currents in the VM. However, large capacitances are necessary to avoid the resonance, resulting in increased circuit volume. A compromise design guideline is

$$2f_s > f_r = \frac{1}{2\pi\sqrt{\frac{L_{\rm kg}}{N^2}C_i}} \tag{13}$$

where C_i is the capacitance (i is the subscript number of shaded substring). For $N = 5.5$ and $L_{kg} = 7.8\,\mu$H of the designed transformer (see Table I) at $f_s = 20$ kHz, (13) produces $C_i > 61.4\,\mu$F. Thus, C_i is determined to be 66 μF (=3 × 22 μF).

IV. CONTROL STRATEGY

As mentioned in Section II-A, there are two control degrees of freedom in qZSIs, and conventional qZSIs in energy storage or PV applications utilize d_{st} and M to control input and output powers independently [49], [51]. The proposed integrated qZSI also utilizes d_{st} and M to realize MPPT and DPP function simultaneously.

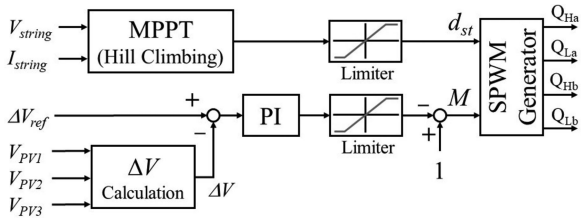

Fig. 12. Control block diagram of ΔV-controlled equalization and MPPT for integrated qZSI.

As mentioned in Section III-C, the operation criterion of the DPP converter in the integrated qZSI depends on $V_{\rm dc}$ or M. Currents for shaded substrings are supplied only when (10) is satisfied. In other words, currents might unnecessarily flow even under unshaded conditions if (10) is improperly fulfilled. Therefore, $V_{\rm dc}$ should be properly regulated by adjusting M depending on shading conditions so that currents are supplied only for shaded substrings under shaded conditions. To this end, $V_{\rm dc}$ needs to be higher and lower than $N(V_{PV} + 2V_f)$ under shaded and unshaded conditions, respectively.

The control block diagram for the integrated qZSI is shown in Fig. 12. It is noted that the control framework for grid synchronization is not included for the sake of clarity. The MPPT control is performed by adjusting d_{st}. Meanwhile, M is manipulated to control the VM-based DPP converter properly. In order to supply currents only for shaded substrings under partial shading conditions, the current sensorless ΔV-controlled equalization strategy is employed [36]. The voltage difference ΔV between the maximum and minimum voltages among $V_{PV1} - V_{PV3}$ is calculated and regulated to be a constant value of $\Delta V_{\rm ref}$ so that only shaded substrings receive equalization currents from the VM-based DPP converter. Under partial shading conditions, ΔV tends to be large, and the output of the proportional-integral (PI) controller grows, consequently reducing M. Hence, according to (10), $V_{\rm dc}$ is controlled to be high under partial-shading conditions. Conventional qZSIs were thoroughly analyzed to get its transfer function [20], [49]. However, deriving a transfer function of the VM-based DPP converter in the proposed integrated qZSI is a daunting challenge as it operates with four operation modes (see Figs. 9 and 10) and contains numerous additional state variables, such as $i_{\rm Lkg}$, $i_{\rm Lmg}$, and voltages of C_1–C_3 and C_{pv1}–C_{pv3}. Given that partial-shading conditions do not change rapidly, PI parameters for the ΔV-controlled equalization loop are determined with trial-and-error basis so that its gain in a high-frequency region can be low enough to ensure the stability.

Images of the ΔV-controlled equalization strategy are illustrated in Fig. 13. Fig. 13(a) deals with the case that PV_1 is partially shaded. The operating point of the unshaded substrings, $\rm PV_2$ and $\rm PV_3$, is determined to be at point A, the intersection point of $I_{\rm string}$, and characteristics of $\rm PV_2$ and $\rm PV_3$. Meanwhile, since ΔV is controlled to be a certain fixed value, the operating point of the shaded substrings $\rm PV_1$ must be ΔV lower than point A. The operating point of $\rm PV_1$ must be on the dashed line L and is determined to be B. The current difference between A and B corresponds to I_1 (i.e., a current supplied to the shaded

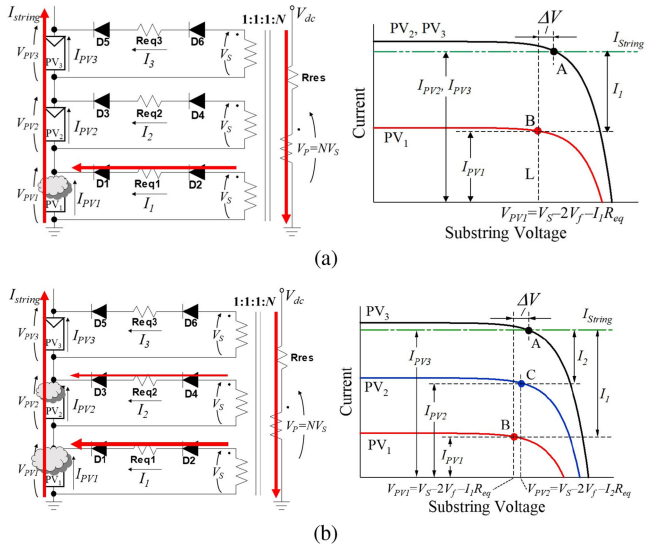

Fig. 13. ΔV-controlled equalization scenarios. (a) PV_1 is shaded. (b) PV_1 and PV_2 are heavily and lightly shaded.

substring from the VM). Although substring voltages cannot be completely equalized, the shaded substring PV_1 can operate at near its MPP by setting ΔV as low as possible.

The substring voltages in the case of Fig. 13(a) are given by

$$\begin{cases} V_{PV1} = V_s - 2V_f - I_1 R_{\rm eq} \\ V_{PV2} = V_{PV3} \geq V_s - 2V_f \end{cases} \tag{14}$$

where $R_{\rm eq}$ is the equivalent resistance, and V_s is the secondary winding voltage. The combination of these two equations produces the voltage difference ΔV between the shaded and unshaded substrings

$$\Delta V = V_{PV3} - V_{PV1} \geq I_1 R_{\rm eq}. \tag{15}$$

This equation suggests that the value of $\Delta V_{\rm ref}$ needs to be determined with considering $R_{\rm eq}$ and the largest expected equalization current under partial shading conditions. To minimize the voltage difference and to satisfactorily equalize substring voltages, $\Delta V_{\rm ref}$ should be set to be as small as possible with ensuring a margin for noise and double-line frequency ripples. If this equation is violated, currents unnecessarily flow toward unshaded substrings, resulting in increased processing power as well as losses in the VM. The value of ΔV for the ΔV-controlled equalization strategy will be determined from the experimentally obtained $R_{\rm eq}$ (see Section V-B).

Fig. 13(b) illustrates the case that PV_1 and PV_2 are heavily and lightly shaded condition. Both PV_1 and PV_2 receive currents from the DPP converter. The current supplied to PV_1, I_1, is larger than that for PV_2, I_2, causing a larger voltage drop across $R_{\rm eq}$ for PV_1 in the form of $I_1 R_{\rm eq}$. Therefore, the voltage of the heavily shaded PV_1, V_{PV1}, tends to be lower than V_{PV2} because of the larger voltage drop. The voltage difference ΔV between the maximum and minimum voltages in this case is V_{PV3}–V_{PV1}, and therefore, the operating point of PV_1 must be ΔV lower than point A and is determined to be B. V_{PV2} is between V_{PV1} and V_{PV3}, and the operating point of PV_2 is at C.

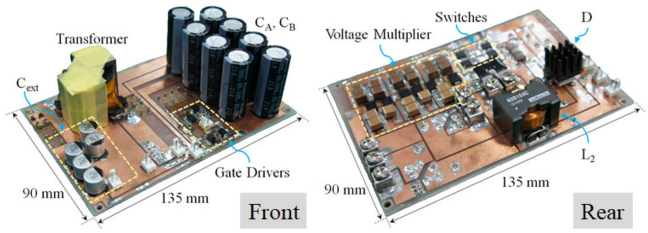

Fig. 14. 150 W prototype of proposed integrated qZSI.

The substring voltages in the case of Fig. 13(b) are expressed as

$$\begin{cases} V_{PV1} = V_S - 2V_f - I_1 R_{\rm eq} \\ V_{PV2} = V_S - 2V_f - I_2 R_{\rm eq} \\ V_{PV3} \geq V_S - 2V_f. \end{cases} \tag{16}$$

Since ΔV in the case of Fig. 13(b) is V_{PV3}–V_{PV1}, the rearrangement of (16) produces an equation identical to (15). This fact suggests that the ΔV-controlled strategy can equalize all the substring voltages with an error of ΔV, regardless of shading conditions.

V. Experimental Results

A. Prototype

The operation of the proposed integrated qZSI was verified using the prototype for a standard 72-cell PV panel comprising three substrings. The prototype and its component values are shown in Fig. 14 and Table I. PV MICs are often installed on the back of PV panels, and the proposed integrated qZSI would be installed similarly. This prototype, however, was designed for proof-of-concept, not for practical use. Bulky high-profile components, such as the transformer with an RM14 core, should preferably be replaced with low-profile ones for the integrated qZSI to be installed on the back of PV panels.

TMS320F28335 control card (Texas Instruments) was used for the MPPT and ΔV-controlled equalization. The prototype operated at a switching frequency of 20 kHz. The measured power conversion efficiency under an unshaded condition with $V_{\rm string} = 36$ V was 83–90% in the output power range of 50–160 W.

B. Output Characteristics of VM-Based DPP Converter

The output characteristics of the VM in the integrated qZSI were measured using the experimental setup shown in Fig. 15. Substrings were removed, and an external power supply $V_{\rm ext}$ of 36 V was connected to the input. By directly connecting the variable resistor $R_{\rm var}$ to C_{pv1}, the current-flow-path under the PV_1-shaded condition (see Fig. 10) can be emulated. The output current $I_{\rm Rvar}$ and the voltage across C_{pv1}, V_{PV1}, were measured with manually regulating $V_{\rm dc}$ to be 52, 60, 72, or 90 V. M was fixed to be 0.78, and a load resistance R_o of 100 Ω was connected to the output of the inverter.

The measured output characteristic of the VM-based DPP converter is shown in Fig. 16. V_{PV1} almost linearly decreased

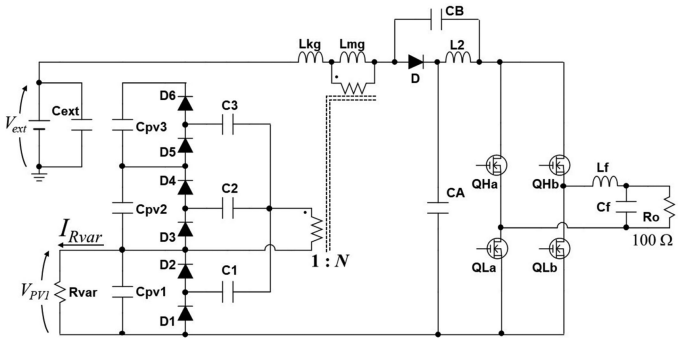

Fig. 15. Experimental setup to measure output characteristics of VM-based DPP converter.

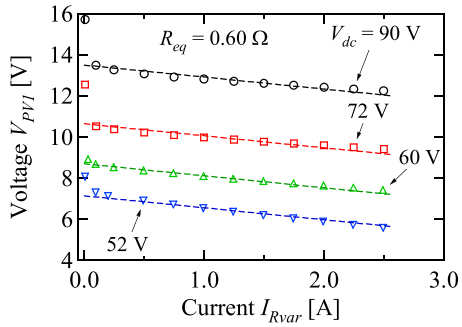

Fig. 16. Measured output characteristics of VM-based DPP converter.

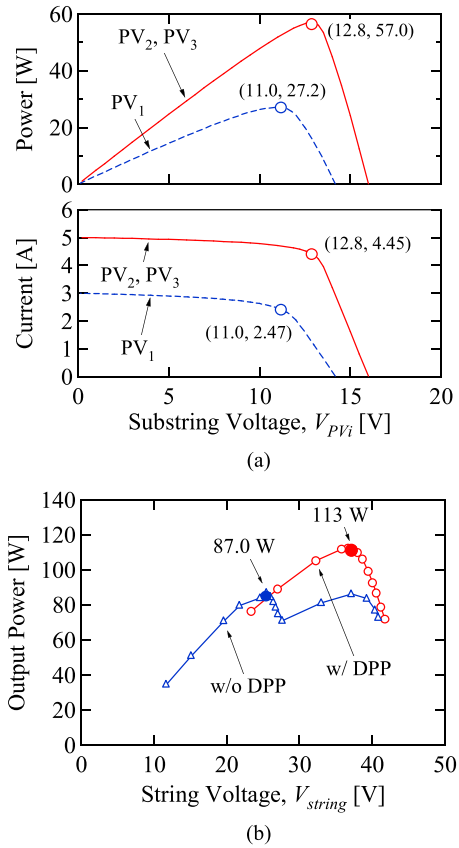

Fig. 17. (a) Substring characteristics, (b) string characteristics with/without DPP function.

with I_{Rvar}. Slopes of the measured characteristics were independent on V_{dc}, and R_{eq} was determined to be 0.60 Ω.

C. String Characteristics Under Partial Shading Condition

A partial shading condition was mimicked using solar array simulators (E4361A, Keysight Technologies). Individual substring characteristics used for the experiments are shown in Fig. 17(a). PV_2 and PV_3 were unshaded, while PV_1 was shaded. The string power available in the ideal case under this partial shading condition was 141.2 W (=27.2 W + 57.0 W × 2). The current difference between the shaded and unshaded substrings was approximately 2.0 A in this case, and R_{eq} was determined to be 0.60 Ω from the measured characteristics of the VM (see Fig. 16). Accordingly, ΔV_{ref} for the current sensorless equalization was set to be 2.0 V to fulfill (15) with considering the influence of noise and leaving enough margin. M was manipulated to achieve ΔV-controlled equalization, while d_{st} was fixed to be 0.2 and the load resistance R_o was manually varied in order to sweep the string characteristics.

The measured inverter output power characteristics as a function of string voltage with/without the DPP function are shown and compared in Fig. 17(b). In the case of without the DPP function, the secondary winding was opened to disable the operation of the VM. Without the DPP converter, two power point maxima (a local and global MPPs) were observed, and the maximum power available at the inverter output was merely 87.0 W at $V_{\mathrm{string}} = 25.5$ V. With the DPP function of the integrated qZSI, on the other hand, the local MPP disappeared, and the maximum output power increased to as high as 113 W at $V_{\mathrm{string}} = 36.7$ V. The available power at the inverter output increased by 30%, and 80% of the ideal string power (=113 W/141.2 W) could be delivered to the output port. Given that the power conversion efficiency of the prototype was 83–90% in the range of 50–160 W, the string was utilized well even under this partial shading condition, demonstrating the DPP function of the integrated qZSI. At $V_{\mathrm{string}} = 36.7$ V with $d_{st} = 0.2$, V_{dc}, V_{CA}, and V_{CB} were measured to be 61.6, 48.7, and 12.0 V, respectively, agreeing well with the theoretical values of (7) and (8).

The measured key operation waveforms at the string's maximum power point of $V_{\mathrm{string}} = 36.7$ V are shown in Fig. 18(a). These waveforms matched well with the theoretical ones shown in Fig. 8. The measured v_o and v_{dc} are shown in Fig. 18(b). v_{dc} swung while generating ac voltage with an rms value of 36 V. These results demonstrated that the proposed integrated qZSI can produce ac output voltage with precluding the negative issues of partial shading.

D. MPPT Under Partial Shading Condition

The experimental MPPT test employing the proposed control strategy was performed emulating a partial shading condition. From the experimentally obtained R_{eq} of 0.60 Ω (see Fig. 16), ΔV_{ref} was determined to be 2.0 V for an equalization current

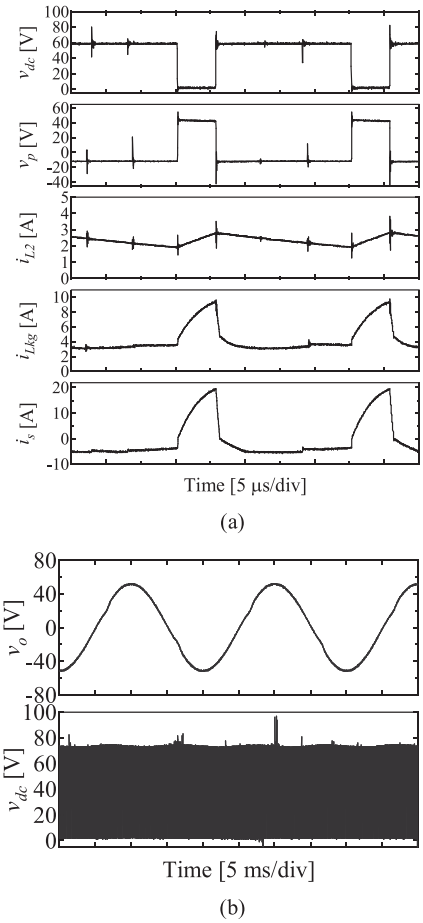

Fig. 18. Measured waveforms at string's MPP. (a) Key waveforms. (b) v_o and $v_{\rm dc}$.

TABLE II
KEY PARAMETERS OF SUBSTRING CHARACTERISTICS IN MPPT TEST

	V_{mp} [V]	V_{oc} [V]	I_{mp} [A]	I_{sc} [A]	P_{MPP} [W]
PV_1 (Shaded)	11	14	0.95	1.0	10.5
PV_2, PV_3 (Unshaded)	12.4	16	1.9	2.0	23.6

of 1.0 A with considering a margin for noise and double-line frequency ripple. ΔV of substring voltages was regulated to be 2.0 V by manipulating M, while the MPP of the string was tracked using the hill climbing algorithm with a duty cycle perturbation Δd_{st} of 0.2%. The sampling interval for the MPPT was set to be 2.0 s, which is hundred times greater than the line frequency period of 20 ms, so that the MPPT operation is not affected by the line frequency of 50 Hz. The key parameters of substring characteristics used for the MPPT test are listed in Table II. The maximum powers of shaded and unshaded substrings were 10.5 and 23.6 W, respectively, and the available maximum string power was 57.7 W in this condition.

The experimental results are shown in Fig. 19. The voltage difference between the shaded and unshaded substrings was controlled to be about 2.0 V, though substring voltages fluctuated due to the duty cycle perturbation. The extracted power

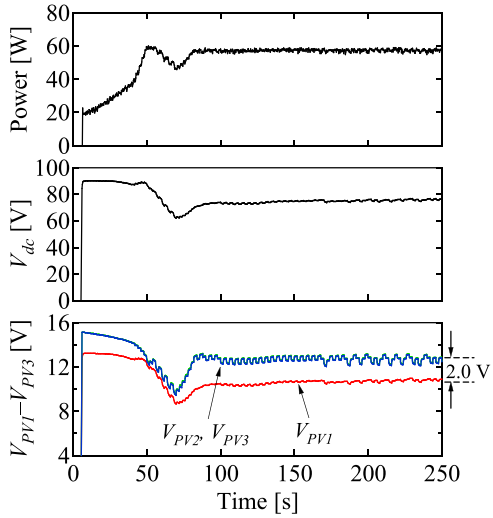

Fig. 19. Experimental results of MPPT with ΔV control.

reached around 57.0 W after the operation came to the steady state, demonstrating the integrated functions of the MPPT and preclusion of decreased power yield by partial shading.

VI. SYSTEM EFFICIENCY COMPARISON

As depicted in Fig. 3, PV systems consist of multiple converters and therefore should be evaluated and compared based on system efficiencies, not converter efficiencies alone. This section presents the comparison between the proposed integrated qZSI system and several representative conventional DPP converters for PV panels comprising three substrings, as shown in Table III. DPP converter efficiencies are a power conversion efficiency of a DPP converter alone. Irradiance conditions represent relative values of short-circuit currents or maximum powers of individual three substrings. The extraction efficiency is defined as a ratio of an extracted power to an ideal panel power under partial shading conditions. System efficiencies were determined with a premise that a qZSI with a power conversion efficiency of 86% was employed for all conventional DPP systems—the 86% efficiency was equivalent to the measured efficiency of the proposed integrated qZSI under unshaded conditions.

Extraction efficiencies of conventional DPP systems are reportedly higher than 90%, depending on topologies and irradiance conditions, and their system efficiencies are around 83%. Meanwhile, the measured system efficiency of the proposed integrated qZSI is 80% (see Section V-C). The inferior system efficiency is chiefly attributable to that the individual performances as a qZSI and DPP converter cannot be optimized due to the integration, as discussed in Section II-C. Furthermore, with the ΔV-controlled equalization strategy, the residual voltage difference ΔV remains even with the DPP function, impairing the system efficiency. Thus, the proposed integrated qZSI is considered better suitable for applications where the system simplification and cost reduction are prioritized over system efficiency enhancement, as mentioned in Section II-C.

TABLE III
SYSTEM EFFICIENCY COMPARISON

Topology	Architecture	Control	DPP Converter Efficiency	Irradiance Condition	Extraction Efficiency	System Efficiency
Resonant SCC [30]	Adjacent Substring [Fig. 2(a)]	Voltage Equalization	99%	100%, 100%, 60%	98.0%	84.3%
Multi-Stacked Buck-Boost Converter [35]	String-to-substring [Fig. 2(b)]	Voltage Equalization	90%	100%, 66%, 33%	91.6%	78.8%
Flyback Converter [39]	String-to-substring [Fig. 2(c)]	Voltage Equalization	90%	100%, 100%, 60%	96.3%	82.8%
Flyback Converter [41]	Substring-to-IP [Fig. 2(e)]	dMPPT	94%	100%, 100%, 50%	98.0%	84.3%
Flyback Converter [42]	Substring-to-IP [Fig. 2(e)]	Voltage Equalization	Not Reported	100%, 75%, 50%	96.5%	83.0%
Proposed	Integrated qZSI (Fig. 4)	Voltage Equalization	N/A	100%, 100%, 60%	N/A	80.0%

VII. CONCLUSION

A novel PV MIC based on cascaded qZSI with DPP capability has been proposed in this paper. The proposed qZSI can be derived by integrating a traditional qZSI and VM-based DPP converter into a single unit with sharing active switches and magnetic components, realizing the simplified system and circuit. The operational analysis revealed that two control freedoms of ST duty cycle d_{st} and modulation index M can be utilized to simultaneously perform the MPPT and DPP function, respectively.

The control strategy for the integrated qZSI has also been presented. MPPT is performed by adjusting d_{st}, while M is manipulated based on the ΔV-controlled equalization strategy, with which a voltage difference between shaded and unshaded substrings is controlled to be a certain fixed value so that partial shading issues are prevented by the DPP converter.

The 150 W prototype of the integrated qZSI was built for a standard 72-cell PV panel comprising three substrings. Experimental tests were performed emulating partial shading conditions. The extractable maximum power from the partially shaded panel increased by 30% under a certain condition, demonstrating the DPP function of the integrated qZSI. With the proposed control strategy, the MPP was properly tracked with regulating ΔV to be a fixed value, demonstrating the integrated functions of MPPT and DPP.

REFERENCES

[1] D. Leuenberger and J. Biela, "PV-module-integrated AC inverter (AC module) with subpanel MPP tracking," *IEEE Trans. Power Electron.*, vol. 32, no. 8, pp. 6105–6118, Aug. 2017.

[2] C. Y. Liao, W. S. Lin, Y. M. Chen, and C. Y. Chou, "A PV microinverter with PV current decoupling strategy," *IEEE Trans. Power Electron.*, vol. 32, no. 8, pp. 6544–6557, Aug. 2017.

[3] D. Meneses, O. Garcia, P. Alou, J. A. Oliver, and J. A. Cobos, "Grid-connected forward microinverter with primary-parallel secondary-series transformer," *IEEE Trans. Power Electron.*, vol. 30, no. 9, pp. 4819–4830, Sep. 2015.

[4] F. Z. Peng, "Z source inverter," *IEEE Trans. Ind. Appl.*, vol. 39, no. 2, pp. 504–510, Mar./Apr. 2003.

[5] Y. Huang, M. Shen, F. Z. Peng, and J. Wang, "Z-source inverter for residential photovoltaic systems," *IEEE Trans. Power Electron.*, vol. 21, no. 6, pp. 1776–1782, Nov. 2006.

[6] O. Husev *et al.*, "Comparison of impedance-source networks for two and multilevel buck–boost inverter applications," *IEEE Trans. Power Electron.*, vol. 31, no. 11, pp. 7564–7579, Nov. 2016.

[7] M. Hanif, M. Basu, and K. Gaughan, "Understanding the operation of a Z-source inverter for photovoltaic application with a design example," *IET Power Electron.*, vol. 4, no. 3, pp. 278–287, Mar. 2009.

[8] C. J. Gajanayake, F. L. Luo, H. B. Gooi, P. L. So, and L. K. Siow, "Extended-boost Z-Source inverters," *IEEE Trans. Power Electron.*, vol. 25, no. 10, pp. 2642–2652, Oct. 2010.

[9] W. Mo, P. C. Loh, and F. Blaabjerg, "Asymmetrical Γ-source inverters," *IEEE Trans. Ind. Electron.*, vol. 61, no. 2, pp. 637–647, Feb. 2014.

[10] M. Zhu, K. Yu, and F. L. Luo, "Switched inductor Z-source inverter," *IEEE Trans. Power Electron.*, vol. 25, no. 8, pp. 2150–2158, Aug. 2010.

[11] D. Li, P. C. Loh, M. Zhu, F. Gao, and F. Blaabjerg, "Generalized multicell switched-inductor and switched-capacitor Z-source inverters," *IEEE Trans. Power Electron.*, vol. 28, no. 2, pp. 837–848, Feb. 2013.

[12] A. V. Ho, T. W. Chun, and H. G. Kim, "Extended boost active-switched-capacitor/switched-inductor quasi-Z-source inverters," *IEEE Trans. Power Electron.*, vol. 30, no. 10, pp. 5681–5690, Oct. 2015.

[13] W. Qian, F. Z. Peng, and H. Cha, "Trans-Z-source inverters," *IEEE Trans. Power Electron.*, vol. 26, no. 12, pp. 3453–3463, Dec. 2011.

[14] M. K. Nguen, Y. C. Lim, and S. J. Park, "Improved trans-Z-source inverter with continuous input current and boost inversion capability," *IEEE Trans. Power Electron.*, vol. 28, no. 10, pp. 4500–4510, Oct. 2013.

[15] M. K. Nguen, Y. C. Lim, and Y. G. Kim, "TZ-source inverters," *IEEE Trans. Ind. Electron.*, vol. 60, no. 12, pp. 5686–5695, Dec. 2013.

[16] P. C. Loh and F. Blaabjerg, "Magnetically coupled impedance-source inverters," *IEEE Trans. Ind. Appl.*, vol. 49, no. 5, pp. 2177–2187, Sep./Oct. 2013.

[17] Y. Zhou and W. Huang, "Single-stage boost inverter with coupled inductor," *IEEE Trans. Power Electron.*, vol. 27, no. 4, pp. 1885–1893, Apr. 2012.

[18] S. S. Nag and S. Mishra, "A coupled inductor based high boost inverter with sub-unity turns-ratio range," *IEEE Trans. Power Electron.*, vol. 31, no. 11, pp. 7534–7543, Nov. 2016.

[19] Y. Zhou, L. Liu, and H. Li, "A high-performance photovoltaic module-integrated converter (MIC) based on cascaded quasi-Z-source inverters (qZSI) using eGaN FETs," *IEEE Trans. Power Electron.*, vol. 28, no. 6, pp. 2727–2738, Jun. 2013.

[20] D. Sun, B. Ge, W. Liang, H. Abu-Rub, and F. Z. Peng, "An energy stored quasi-Z-source cascade multilevel inverter-based photovoltaic power generation system," *IEEE Trans. Ind. Electron.*, vol. 62, no. 9, pp. 5458–5467, Sep. 2015.

[21] S. M. MacAlpine, R. W. Erickson, and M. J. Brandemuehl, "Characterization of power optimizer potential to increase energy capture in photovoltaic systems operating under nonuniform conditions," *IEEE Trans. Power Electron.*, vol. 28, no. 6, pp. 2936–2945, Jun. 2013.

[22] H. Jeong, H. Lee, Y. C. Liu, and K. A. Kim, "Review of differential power processing converters techniques for photovoltaic applications," *IEEE Trans. Energy Conversion*, vol. 34, no. 1, pp. 351–360, Mar. 2019.

[23] H. J. Bergveld *et al.*, "Module-level dc/dc conversion for photovoltaic systems: The delta-conversion concept," *IEEE Trans. Power Electron.*, vol. 28, no. 4, pp. 2005–2013, Apr. 2013.

[24] M. S. Zaman *et al.*, "A cell-level differential power processing IC for concentrating-PV systems with bidirectional hysteretic current-mode control and closed-loop frequency regulation," *IEEE Trans. Power Electron.*, vol. 30, no. 12, pp. 7230–7244, Dec. 2015.

[25] P. S. Shenoy, K. A. Kim, B. B. Johnson, and P. T. Krein, "Differential power processing for increased energy production and reliability of photovoltaic systems," *IEEE Trans. Ind. Power Electron.*, vol. 28, no. 6, pp. 2968–2979, Jun. 2013.
[26] S. Qin, S. T. Cady, A. D. D. García, and R. C. N. P. Podgurski, "A distributed approach to maximum power point tracking for photovoltaic submodule differential power processing," *IEEE Trans. Power Electron.*, vol. 30, no. 4, pp. 2024–2040, Apr. 2015.
[27] S. Qin, C. B. Barth, and R. C. N. P. Podgurski, "Enhancing microinverter energy capture with submodule differential power processing," *IEEE Trans. Power Electron.*, vol. 31, no. 5, pp. 3575–3585, May 2016.
[28] T. Shimizu, O. Hashimoto, and G. Kimura, "A novel high-performance utility-interactive photovoltaic inverter system," *IEEE Trans. Power Electron.*, vol. 18, no. 2, pp. 704–711, Mar. 2003.
[29] T. Shimizu, M. Hirakata, T. Kamezawa, and H. Watanabe, "Generation control circuit for photovoltaic modules," *IEEE Trans. Power Electron.*, vol. 16, no. 3, pp. 293–300, May 2001.
[30] J. T. Stauth, M. D. Seeman, and K. Kesarwani, "Resonant switched-capacitor converters for sub-module distributed photovoltaic power management," *IEEE Trans. Power Electron.*, vol. 28, no. 3, pp. 1189–1198, Mar. 2013.
[31] P. K. Peter and V. Agarwal, "Current equalization in photovoltaic strings with module integrated ground-isolated switched capacitor DC–DC converters," *IEEE J. Photovoltaics.*, vol. 4, no. 2, pp. 669–678, Mar. 2014.
[32] A. Blumenfeld, A. Cervera, and M. M. Peretz, "Enhanced differential power processor for PV systems: Resonant switched-capacitor gyrator converter with local MPPT," *IEEE J. Emerg. Sel. Topics Power Electron.*, vol. 2, no. 4, pp. 883–892, Dec. 2014.
[33] M. Uno and A. Kukita, "PWM converter integrating switched capacitor converter and series-resonant voltage multiplier as equalizers for photovoltaic modules and series-connected energy storage cells for exploration rovers," *IEEE Trans. Power Electron.*, vol. 32, no. 11, pp. 8500–8513, Nov. 2017.
[34] J. Du, R. Xu, X. Chen, Y. Li, and J. Wu, "A novel solar panel optimizer with self-compensation for partial shadow condition," in *Proc. IEEE Applied Power Electron. Conf. Expo., APEC*, 2013, pp. 92–96.
[35] M. Uno and A. Kukita, "Single-switch voltage equalizer using multistacked buck-boost converters for partially-shaded photovoltaic modules," *IEEE Trans. Power Electron.*, vol. 30, no. 6, pp. 3091–3105, Jun. 2015.
[36] M. Uno and A. Kukita, "Current sensorless equalization strategy for a single-switch voltage equalizer using multistacked buck–boost converters for photovoltaic modules under partial shading," *IEEE Trans. Ind. Appl.*, vol. 53, no. 1, pp. 420–429, Jan./Feb. 2017.
[37] M. Uno and A. Kukita, "Two-switch voltage equalizer using an LLC resonant inverter and voltage multiplier for partially-shaded series-connected photovoltaic modules," *IEEE Trans. Ind. Appl.*, vol. 51, no. 2, pp. 1587–1601, Mar./Apr. 2015.
[38] M. Uno and A. Kukita, "Single-switch single-magnetic PWM converter integrating voltage equalizer for partially-shaded photovoltaic modules in standalone applications," *IEEE Trans. Power Electron.*, vol. 33, no. 2, pp. 1259–1270, Feb. 2018.
[39] C. Olalla, D. Clement, M. Rodríguez, and D. Makisimović, "Architectures and control of submodule integrated dc–dc converters for photovoltaic applications," *IEEE Trans. Power Electron.*, vol. 28, no. 6, pp. 2980–2997, Jun. 2013.
[40] C. Olalla, C. Deline, D. Clement, Y. Levron, M. Rodríguez, and D. Makisimović, "Performance of power limited differential power processing architectures in mismatched PV systems," *IEEE Trans. Power Electron.*, vol. 30, no. 2, pp. 618–631, Feb. 2015.
[41] R. Bell and R. C. N. P. Podgurski, "Decoupled and distributed maximum power point tracking of series-connected photovoltaic submodules using differential power processing," *IEEE J. Emerg. Sel. Topics Power Electron.*, vol. 3, no. 4, pp. 881–891, Dec. 2015.
[42] Y. Levron, D. R. Clement, B. Choi, C. Olalla, and D. Maksimovic, "Control of submodule integrated converters in the isolated-port differential power-processing photovoltaic architecture," *IEEE J. Emerg. Sel. Topics Power Electron.*, vol. 2, no. 4, pp. 821–832, Dec. 2014.
[43] G. Chu, H. Wen, L. Jiang, Y. Hu, and X. Li, "Bidirectional flyback based isolated-port submodule differential power processing optimizer for photovoltaic applications," *Solar Energy*, vol. 158, pp. 929–940, Oct. 2017.
[44] Y. T. Jeon, H. Lee, K. A. Kim, and J. H. Park, "Least power point tracking method for photovoltaic differential power processing systems," *IEEE Trans. Power Electron.*, vol. 32, no. 3, pp. 1941–1951, Mar. 2017.
[45] T. Shinohara and M. Uno, "Micro-inverter based on quasi-Z-source inverter integrating switchless voltage equalizer for photovoltaic panels under partial shading," in *Proc. Int. Future Energy Electron. Conf. (IFEEC), ECCE-Asia*, Jun. 2017, pp. 2013–2018.
[46] Y. Zhou and H. Li, "Analysis and suppression of leakage current in cascaded-multilevel-inverter-based PV systems," *IEEE Trans. Power Electron.*, vol. 29, no. 10, pp. 5265–5277, Oct. 2014.
[47] J. Kan, Y. Wu, L. Qin, and S. Luo, "Integrated double dual-MOSFETs photovoltaic micro-inverter with current-source characteristic," in *Proc. Int. Future Energy Electron. Conf. (IFEEC) ECCE-Asia*, 2017, pp. 134–139.
[48] D. R. Nayanasiri, D. M. Vilathgamuwa, and D. L. Maskell, "Half-wave cycloconverter-based photovoltaic microinverter topology with phase-shift power modulation," *IEEE Trans. Power Electron.*, vol. 28, no. 6, pp. 2700–2710, Jun. 2013.
[49] B. Ge *et al.*, "An energy-stored quasi-Z-source inverter for application to photovoltaic power system," *IEEE Trans. Ind. Electron.*, vol. 60, no. 10, pp. 4468–4481, Oct. 2013.
[50] M. K. Nguyen, Y. C. Lim, and S. J. Park, "A comparison between single-phase quasi-Z-source and quasi-switched boost inverters," *IEEE Trans. Ind. Electron.*, vol. 62, no. 10, pp. 6336–6344, Oct. 2015.
[51] F. Z. Peng, M. Shen, and K. Holland, "Applications of Z-source inverter for traction drive of fuel cell—battery hybrid electric vehicles," *IEEE Trans. Power Electron.*, vol. 22, no. 3, pp. 1054–1061, May 2007.

Masatoshi Uno (M'06) was born in Japan in 1979. He received the B.E. and M.E. degrees, both in electrical engineering from Doshisha University, Kyoto, Japan, and the Ph.D. degree in space and astronautical science from the Graduate University for Advanced Studies, Hayama, Japan, in 2002, 2004, and 2012, respectively.

In 2004, he joined Japan Aerospace Exploration Agency, Sagamihara, Japan, where he developed spacecraft power systems including battery, photovoltaic, and fuel cell systems. In 2014, he joined the Department of Electrical and Electronics Engineering, Ibaraki University, Ibaraki, Japan, where he is currently an Associate Professor of electrical engineering. His research interests include switching power converters for renewable energy systems, life evaluation for EDLCs and lithium-ion batteries, and development of spacecraft power systems.

Dr. Uno received the Isao Takahashi Power Electronics Award in 2018.

Toshiki Shinohara was born in 1992. He received the B.E. and M.S. degrees in electrical and electronics engineering from Ibaraki University, Ibaraki, Japan, in 2016 and 2018, respectively.

He is currently with TOYOTA Corporation. His research interests include dc–dc converters and inverters for photovoltaic systems.